AIAA JOURNAL
Vol. 48, No. 11, November 2010

Technical Notes

Aerodynamic Performance of Cambered Heaving Airfoils

Joel E. Guerrero*
University of Genoa, 16145 Genoa, Italy

DOI: 10.2514/1.J050036

Nomenclature

c	=	airfoil mean chord
c_d	=	instantaneous drag coefficient
c_l	=	instantaneous lift coefficient
$\bar{c}_l$	=	time average lift coefficient
c_P	=	instantaneous input power coefficient
$\bar{c}_P$	=	time average input power coefficient
c_t	=	instantaneous thrust coefficient ($c_t = -c_d$)
$\bar{c}_t$	=	time average thrust coefficient
f	=	heaving frequency
h_a	=	heaving amplitude
k	=	reduced frequency, $\pi f c/U_\infty$
Re	=	Reynolds number, $U_\infty c/\nu$
St	=	Strouhal number, $2fh_a/U_\infty$
t	=	time
U_∞	=	freestream velocity
η	=	propulsive efficiency, $\bar{c}_t/\bar{c}_P$
ν	=	fluid kinematic viscosity
ρ	=	fluid density

I. Introduction

TRADITIONALLY, most flapping airfoil experimental and numerical studies have been limited to NACA symmetrical airfoils, or to a lesser extent, elliptical airfoils [1–3]. In flapping airfoil studies, the effect of airfoil geometry (in particular airfoil cambering) has not been sufficiently investigated, even though it is crucial for lift generation. The reason why this area has not been studied enough is that most researchers are chiefly interested in thrust generation and propulsion efficiency. In this technical note, we conduct a parametric study to assess the effect of airfoil cambering on the aerodynamic performance of rigid heaving airfoils, independently of any possible practical applications.

II. Solution Methodology

Hereafter, we briefly outline the methodology used to solve the governing equations on moving structured overlapping grids. The complete description of the numerical method and the gridding method can be found in the papers by Henshaw [4] and Chesshire and Henshaw [5], respectively. For our problem, the governing equations to be solved are the laminar incompressible Navier–Stokes equations in their velocity-pressure formulation [4,6]:

$$\frac{\partial \mathbf{u}}{\partial t} + \mathbf{u}\cdot\nabla\mathbf{u} = \frac{-\nabla p}{\rho} + \nu\nabla^2\mathbf{u} \quad \text{for } \mathbf{x}\in D, \qquad t>0 \tag{1}$$

$$\frac{\nabla^2 p}{\rho} + \nabla u\cdot\mathbf{u}_x + \nabla v\cdot\mathbf{u}_y + \nabla w\cdot\mathbf{u}_z = 0 \quad \text{for } \mathbf{x}\in D, \qquad t>0 \tag{2}$$

with the following boundary and initial conditions

$$B(\mathbf{u},p) = \mathbf{g} \quad \text{for } \mathbf{x}\in \partial D, \qquad t>0 \tag{3}$$

$$\nabla\cdot\mathbf{u} = 0 \quad \text{for } \mathbf{x}\in \partial D, \qquad t>0 \tag{4}$$

$$\mathbf{u}(\mathbf{x},t_0) = \mathbf{u}_0(\mathbf{x}) \quad \text{for } \mathbf{x}\in D, \qquad t_0 = 0 \tag{5}$$

Equations (1–5) are solved in logically rectangular grids in the transformed computational space C, using second-order centered finite difference approximations on structured overlapping grids. Then, the discretized equations are integrated in time using a semi-implicit multistep method. This method uses a Crank–Nicolson scheme for the viscous terms and a second-order Adams–Bashforth/Adams–Moulton predictor-corrector approach for the convective terms. This yields a second-order accurate in space and time numerical scheme.

For moving overlapping grids, Eqs. (1) and (2) are expressed in a reference frame that moves with the component grid as follows:

$$\frac{\partial \mathbf{u}}{\partial t} + [(\mathbf{u}-\dot{\mathbf{G}})\cdot\nabla]\mathbf{u} = \frac{-\nabla p}{\rho} + \nu\nabla^2\mathbf{u} \quad \text{for } \mathbf{x}\in D, \qquad t>0 \tag{6}$$

$$\frac{\nabla^2 p}{\rho} + \nabla u\cdot\mathbf{u}_x + \nabla v\cdot\mathbf{u}_y + \nabla w\cdot\mathbf{u}_z = 0 \quad \text{for } \mathbf{x}\in D, \qquad t>0 \tag{7}$$

where $\dot{\mathbf{G}}$ is the rate of change of the position of a given set of grid points $\mathbf{x}_P$ in the physical space P (grid velocity). It is important to note that the new governing equations expressed in the moving reference frame must be accompanied by proper boundary conditions; for a moving body with a corresponding moving no-slip wall, only one constraint may be applied. This constrain corresponds to the velocity on the wall, given by

$$\mathbf{u}(\mathbf{x}_P|_{\text{wall}}, t) = \dot{\mathbf{G}}(\mathbf{x}_P|_{\text{wall}}, t) \tag{8}$$

To assemble the overlapping grid system G and solve the governing equations the Overture† framework is used. The large, sparse nonlinear system of equations arising from the discretization of the incompressible Navier-Stokes equations is solved using the PETSc‡ library, which was interfaced with Overture. The system of nonlinear equations is then solved using a Newton–Krylov iterative method, in combination with a suitable preconditioner.

Received 1 July 2009; revision received 12 August 2010; accepted for publication 12 August 2010.

*Postdoctoral Fellow, Department of Civil, Environmental and Architectural Engineering, DICAT, Via Montallegro 1, Italy 16145; joel.guerrero@unige.it. Senior Member AIAA.

†Additional data available online at https://computation.llnl.gov/casc/Overture/ [Accessed Sept. 2010].

‡Additional data and for an animation available at the author's web site: http://www.dicat.unige.it/guerrero/flappingsimulationsnew.html. [Accessed Sept. 2010].

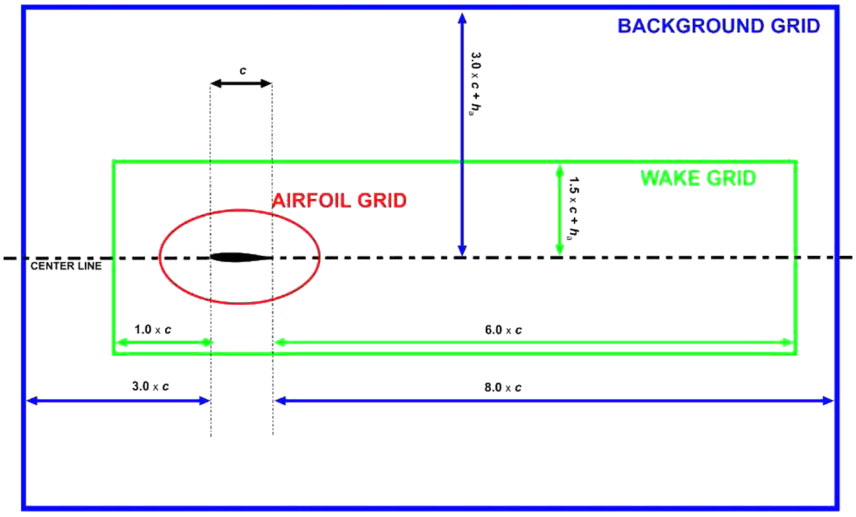

Fig. 1 Overlapping grid system G layout for the heaving airfoil case.

III. Results and Discussion

The overlapping grid system G layout used to conduct this parametric study is shown in Fig. 1. In this figure, the grid size of the background grid (BG) is 200×110 (in the x and y directions), the size of the wake grid (WG) is 400×180 (in the x and y directions), and the size of the airfoil grid (AG) is 300×120 (on the airfoil surface and the direction normal to the airfoil surface, respectively). Here, h_a is assumed to be equal to 0.3. In the case of a bigger or smaller domain, the grid dimensions are scaled to keep the same grid spacing as for this domain. For the AG, the first node normal to the airfoil surface (FST-NW), is located at a distance equal to $0.00005 \times c$ and there are as many as 20 normal points clustered in the direction normal to the airfoil surface (the boundary-layer area). Mesh clustering is also used near the leading and trailing edges, because we expect vortices to be generated in these areas. This overlapping grid system provides grid-independent results and was chosen after conducting an extensive quantitative (force measurements) and qualitative (wake structure resolution) grid refinement study. To conduct this study, we used the grid convergence index (GCI) method as described by Roache [7]. Hereafter, a NACA 0012 airfoil, undergoing a pure heaving motion according to Eq. (9), is considered for different grid sizes, layouts and mesh clustering. Several simulations were run for $St = 0.5$ and $h_a = 0.25$ (thrust production regime) and Re equal to 1500. In Table 1, a detailed description of the three overlapping grid systems used for the GCI study is presented. Table 2 shows the observed values of $\bar{c}_t$ for each grid system described in Table 1. These values are used to compute the observed order of convergence p, the value of the observed quantity at zero grid spacing $f_{h=0}$, the fine grid convergence index GCI_{12} and GCI_{23}, and the constancy of $(\mathrm{GCI}_{23}/\mathrm{GCI}_{12}) \times (1/r^p)$. Based on the GCI index values found, $\bar{c}_t$ is estimated to be 1.5290 with an error band of 0.1946% for grid G_1 and an error band of 0.7879% for grid G_2. Both grids are well within the asymptotic range of convergence as evidenced by the constancy of $(\mathrm{GCI}_{23}/\mathrm{GCI}_{12}) \times (1/r^p)$. After taking into account the computational resources available, CPU time restrictions and solution accuracy; G_2 was chosen as the base overlapping grid system.

The initial conditions used in each heaving airfoil simulation are those of a fully converged solution of the corresponding fixed airfoil case. The left boundary of the BG in Fig. 1 corresponds to an inflow boundary condition ($\mathbf{u} = (1, 0)$, $\partial_{\hat{\mathbf{n}}} p = 0$). The top, bottom and right boundaries of the BG are outflow boundaries (basically vanishing pressure gradient and velocity extrapolated from the interior points). Also, the heaving airfoil has a no-slip boundary condition [$\mathbf{u} = (\dot{\mathbf{G}}_x \dot{\mathbf{G}}_y)$]. The rest of the boundaries are interpolation boundaries. The Reynolds number for all forthcoming heaving airfoil numerical experiments is equal to 1100. The airfoils used for this parametric study are based on the standard NACA four digits series [8], where we simply changed the maximum airfoil cambering and its position. The NACA airfoils used were the following: 0012, 2212, 2412, 2612, 4412, 4612, and 6612. Additionally, we used the high-lift low Reynolds number Selig S1223 airfoil [9]. This latter airfoil was chosen because of its similarities to the Seagull wings' cross section, as observed by Liu et al. [10]. All the computations were checked for proper iterative convergence.

In the numerical experiments carried out hereafter, the airfoil is undergoing time-dependent heaving motion $y(t)$ as follows:

$$y(t) = h_a - h_a \times \cos(2\pi f_h t) \tag{9}$$

Several numerical simulations were performed at three different St values equal to 0.2, 0.3, and 0.4 (in the region of St where the propulsive efficiency η is high [1,11]) and two different values of heaving amplitude h_a, one corresponding to high heaving frequencies f (low heaving amplitudes h_a) and the other corresponding to low heaving frequencies f (high heaving amplitudes h_a). The summary of results is presented in Tables 3–5, where the product $\bar{c}_t \times \bar{c}_l$ represents the driving figure of merit that is used to choose the

Table 2 GCI study results

G_g (Grid system)	$\bar{c}_t$
G_1	1.5267
G_2	1.5195
G_3	1.4905
Order of Convergence p	2.0099
$f_{h=0}$	1.5290
GCI_{12} , %	0.1946%
GCI_{23} , %	0.7879%
$(\mathrm{GCI}_{23}/\mathrm{GCI}_{12}) \times (1/r^p)$	0.9952

Table 1 Description of grids used for the grid refinement study. GSR stands for grid refinement spacing ratio with reference to the airfoil grid AG

G_g(Grid system)	BG	WG	AG	GSR	FST-NW
G_1	240×120	400×180	600×240	1	$0.000025 \times c$
G_2	200×110	400×180	300×120	2	$0.00005 \times c$
G_3	200×110	360×140	150×60	4	$0.0001 \times c$

Table 3 Summary of results for $St = 0.4$, $Re = 1100$

Airfoil type	$h_a(f_h) = 0.1(2.0)$					$h_a(f_h) = 0.3(0.66666)$				
	$\bar{c}_t$	$\bar{c}_P$	η	$\bar{c}_l$	$\bar{c}_t \times \bar{c}_l$	$\bar{c}_t$	$\bar{c}_P$	η	$\bar{c}_l$	$\bar{c}_t \times \bar{c}_l$
NACA 0012	0.8515	7.5748	0.1124	0.0093	0.0079	0.8292	5.3332	0.1554	0.0144	0.0119
NACA 2212	0.9326	7.6910	0.1212	0.0283	0.0263	0.8244	5.3221	0.1549	0.2279	0.1878
NACA 2412	0.9329	7.7209	0.1208	0.1120	0.1044	0.8486	5.3313	0.1591	0.1074	0.0911
NACA 4412	0.9080	7.6433	0.1188	0.4465	0.4054	0.8035	5.2321	0.1535	0.1584	0.1272
NACA 2612	0.9286	7.7304	0.1201	0.2475	0.2298	0.8340	5.3293	0.1565	0.3194	0.2663
NACA 4612	0.8920	7.6356	0.1168	0.7074	0.6310	0.8067	5.2851	0.1526	0.3963	0.3196
NACA 6612	0.8664	7.5440	0.1148	1.1194	0.9698	0.7627	5.1025	0.1494	0.4675	0.3565
Selig S1223	0.7944	7.2373	0.1097	1.4181	1.1265	0.4284	4.4070	0.0972	0.2658	0.1138

Table 4 Summary of results for $St = 0.3$, $Re = 1100$

Airfoil type	$h_a(f_h) = 0.1(1.5)$					$h_a(f_h) = 0.3(0.5)$				
	$\bar{c}_t$	$\bar{c}_P$	η	$\bar{c}_l$	$\bar{c}_t \times \bar{c}_l$	$\bar{c}_t$	$\bar{c}_P$	η	$\bar{c}_l$	$\bar{c}_t \times \bar{c}_l$
NACA 0012	0.3928	2.8441	0.1381	0.0123	0.0048	0.2487	2.0851	0.1193	0.0069	0.0017
NACA 2212	0.4039	2.8998	0.1393	0.0391	0.0157	0.2391	2.1146	0.1130	0.1701	0.0406
NACA 2412	0.4048	2.9115	0.1390	0.2000	0.0809	0.2388	2.1114	0.1131	0.1962	0.0468
NACA 4412	0.3911	2.9078	0.1345	0.4871	0.1905	0.2306	2.0715	0.1113	0.3845	0.0886
NACA 2612	0.4018	2.9051	0.1383	0.3018	0.1212	0.2382	2.1139	0.1126	0.2371	0.0564
NACA 4612	0.3815	2.8886	0.1321	0.6580	0.2510	0.2244	2.0692	0.1084	0.4738	0.1063
NACA 6612	0.3483	2.8655	0.1215	0.9983	0.3477	0.1997	2.0099	0.0993	0.6799	0.1357
Selig S1223	0.3562	2.9019	0.1227	1.0351	0.3687	0.1602	1.7992	0.0890	0.6366	0.1019

Table 5 Summary of results for $St = 0.2$, $Re = 1100$

Airfoil type	$h_a(f_h) = 0.1(1.0)$					$h_a(f_h) = 0.3(0.33333)$				
	$\bar{c}_t$	$\bar{c}_P$	η	$\bar{c}_l$	$\bar{c}_t \times \bar{c}_l$	$\bar{c}_t$	$\bar{c}_P$	η	$\bar{c}_l$	$\bar{c}_t \times \bar{c}_l$
NACA 0012	0.0608	0.8299	0.0733	0.0091	0.0005	0.0386	0.6201	0.0623	0.0081	0.0003
NACA 2212	0.0717	0.8002	0.0896	0.1065	0.0076	0.0480	0.6757	0.0710	0.0198	0.0009
NACA 2412	0.0723	0.7983	0.0906	0.1207	0.0087	0.0462	0.6457	0.0715	0.0656	0.0030
NACA 4412	0.0580	0.8023	0.0723	0.3546	0.0205	0.0381	0.6877	0.0554	0.1883	0.0071
NACA 2612	0.0723	0.7985	0.0906	0.1624	0.0117	0.0495	0.6586	0.0752	0.0891	0.0044
NACA 4612	0.0575	0.7904	0.0727	0.3820	0.0219	0.0361	0.6607	0.0547	0.1708	0.0061
NACA 6612	0.0332	0.7796	0.0425	0.5947	0.0197	0.0106	0.6188	0.0172	0.2046	0.0021
Selig S1223	0.0004	0.8863	0.0004	0.9698	0.0003	-0.049	0.6297	-	0.2196	-

[a]Note: for negative thrust coefficients, the propulsive efficiency η and the product $\bar{c}_t \times \bar{c}_l$ are not shown.

best airfoil for any given heaving configuration. The biggest value of the product $\bar{c}_t \times \bar{c}_l$ represents the best airfoil for the case studied.

Inspecting Table 3 for the case where $h_a = 0.1$, and using the results of the NACA 0012 airfoil as a reference, we observe that the values of $\bar{c}_t$, $\bar{c}_P$ and η do not change much as the maximum airfoil cambering and its position are modified. Conversely, looking at the values of $\bar{c}_l$, we observe that the values increase as we change the maximum airfoil cambering and its position. In fact, we are now producing a positive average lift coefficient $\bar{c}_l$. Similar observations apply for the results presented in Tables 4 and 5. From these results, we can also identify a region of drag production or very little thrust production, for values of St around 0.2 (Table 5). There is also a region of thrust production for values of St higher than 0.2 (Tables 3 and 4). Looking at Tables 3 and 4 and using the product $\bar{c}_t \times \bar{c}_l$ as the main figure of merit, it is found that for low heaving amplitudes (high heaving frequencies) and St equal to 0.3 and 0.4 the best airfoil is the Selig S1223. For high heaving amplitudes (low heaving frequencies) and St equal to 0.3 and 0.4 the best airfoil is the NACA 6612. The product $\bar{c}_t \times \bar{c}_l$ means that for the given heaving configuration, the chosen airfoil has a high acceleration rate, high climb rate and high lift-to-drag ratio.

From the results presented, it can be also observed that very different behaviors of the aerodynamic performance can be obtained between high heaving frequencies and low heaving frequencies. A maximum propulsive efficiency value is obtained at $St = 0.3$ for $h_a = 0.1$, whereas for $h_a = 0.3$ the maximum propulsive efficiency value is obtained for $St = 0.4$. This frequency dependence is due to the leading-edge vortices (LEVs) shedding process, as discussed by Young and Lai [12] and Wang [13]. It is worth mentioning that the results presented by Young and Lai [12] and Wang [13], were obtained for symmetrical airfoils. The results presented in this technical note, extend their observations to nonsymmetrical airfoils.

In flapping airfoil studies it is critical to understand the vortical patterns created by the oscillating airfoil. These are related to drag production in certain cases, but also to thrust production in other cases. In Fig. 2,[§] a comparison of the vorticity field for a NACA 0012 and a Selig S1223 airfoil is presented. Notice that the vorticity field for the S1223 airfoil is no longer symmetric, hence the strength and shedding of the LEVs during the upstroke (recovery stroke) and downstroke (power stroke) are different. The sequence illustrated in this figure is shown for four instants during the upstroke motion. It is worth noting that for the S1223 airfoil, the LEV traveling on the extrados is convected downstream during the upstroke motion and does not interact with the LEV produced in the previous heaving cycle, diffusing as it moves toward the trailing edge; whereas on the intrados, the newly generated LEV interacts with the LEV generated

[§]Additional data and for an animation available at the author's web site: http://www.dicat.unige.it/guerrero/flappingsimulationsnew.html. [Accessed Sept. 2010].

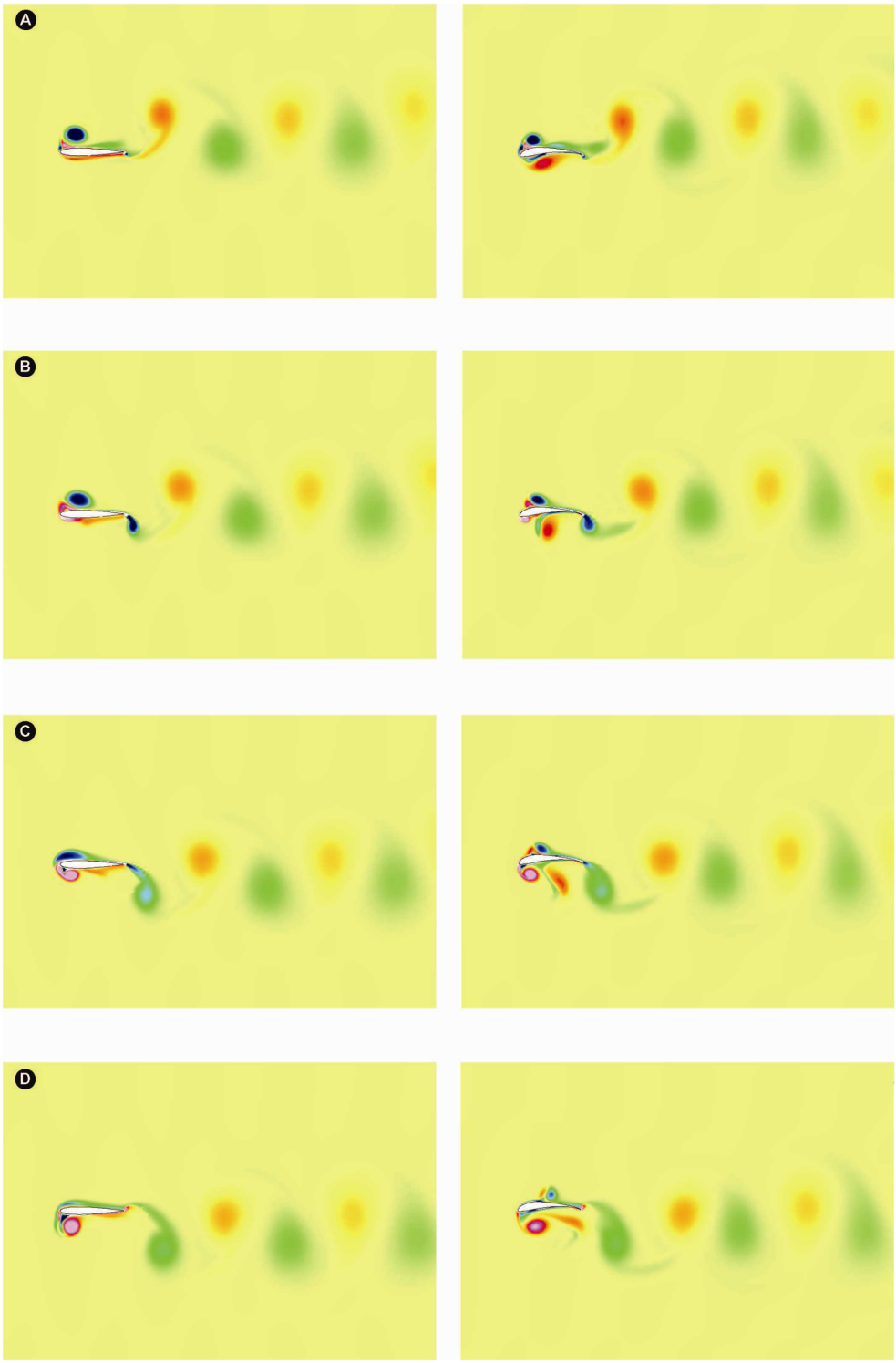

Fig. 2 Comparison of the vorticity field for two airfoils. Left column: NACA 0012 airfoil. Right column: Selig S1223 airfoil. Heaving parameters: $St = 0.4$, $h_a = 0.3$. Part a) $t = 9.0$, b) $t = 9.25$, c) $t = 9.50$, and d) $t = 9.75$.

in the previous stroke, until ultimately it is convected. For the NACA 0012, the LEVs traveling on the intrados and extrados are convected all the way downstream with the same shedding rate and they do not interact with the LEVs generated in the previous heaving cycle.

IV. Conclusions

In this technical note, the effect of airfoil cambering on the aerodynamic performance of heaving airfoils was assessed. It was found that this geometric parameter has a strong influence on the lift coefficient, while it has a smaller impact on the global thrust coefficient and propulsive efficiency, at least in the range of St values where significant and sustained $\bar{c}_t$ was achieved (St higher than 0.3). For values of St around 0.2 (the region of drag production or very little thrust production) this behavior was not observed, probably due to transitional phenomena between drag and thrust producing wakes or LEV shedding due to the airfoil curvature, and further studies should be carried out to explain this behavior. Hence, it seems that thrust production depends more on the heaving parameters (St and k), than on the airfoil shape. On the other hand, lift production is dominated by the airfoil shape, specifically, airfoil cambering. Among all the asymmetric airfoils used, the NACA 6612 airfoil

provides the best aerodynamic performance in terms of the product $\bar{c}_t \times \bar{c}_l$ for high heaving amplitudes (low heaving frequencies). This airfoil generates a high average lift coefficient, which, along thrust generation, are the crucial parameters if interest resides in flapping flight. The S1223 airfoil, which resembles the cross-section of a Seagull wing, provides the best aerodynamic performance in terms of the product $\bar{c}_t \times \bar{c}_l$ at low heaving amplitudes (high heaving frequencies). On the other hand, at high heaving amplitudes (low heaving frequencies), the aerodynamic performance of the S1223 airfoil deteriorated in comparison to the other airfoils, although thrust and positive average lift coefficient were still produced. These observations lead us to conclude that this airfoil is optimum for low heaving amplitudes, and hence for gliding and intermittent flapping flight. This is expected because Seagulls are very good gliders. The results presented also show that nonsymmetrical heaving airfoils exhibit LEV shedding and frequency dependence similar to that of symmetric heaving airfoils.

Finally, the results presented in this technical note are limited to laminar flow. Nevertheless, they provide excellent insight into the aerodynamic performance of cambered rigid heaving airfoils. We envisage the extension of the current study to turbulent flow and laminar separation bubbles. The use of more realistic (nonsymmetrical) flapping kinematics and the use of flexible wings are also foreseen.

Acknowledgments

We acknowledge the financial support of the Marie Curie actions EST project FLUBIO, through grant MEST-CT-2005-020228. The use of the computing facilities at the high-performance computing center of the University of Stuttgart was possible thanks to the support of the HPC-Europa++ project (project number 211437), with the support of the European Community, Research Infrastructure Action of the FP7.

References

[1] Anderson, J., Streitlien, K., Barret, D., and Triantafyllou, M., "Oscillating Foils of High Propulsive Efficiency," *Journal of Fluid Mechanics*, Vol. 360, 1998, pp. 41–72. doi:10.1017/S0022112097008392

[2] Lua, K., Lim, T., Yeo, K., and Oo, G., "Wake-Structure Formation of a Heaving Two-Dimensional Elliptic Airfoil," *AIAA Journal*, Vol. 45, No. 7, 2007, pp. 1571–1583. doi:10.2514/1.25310

[3] Soueid, H., Guglielmini, L., Airiau, C., and Bottaro, A., "Optimization of the Motion of a Flapping Airfoil Using Sensitivity Functions," *Computers and Fluids*, Vol. 38, 2009, pp. 861–874. doi:10.1016/j.compfluid.2008.09.012

[4] Henshaw, W., "A Fourth-Order Accurate Method for the Incompressible Navier-Stokes Equations on Overlapping Grids," *Journal of Computational Physics*, Vol. 113, No. 1, 1994, pp. 13–25. doi:10.1006/jcph.1994.1114

[5] Chesshire, G., and Henshaw, W., "Composite Overlapping Meshes for the Solution of Partial Differential Equations," *Journal of Computational Physics*, Vol. 90, No. 1, 1990, pp. 1–64. doi:10.1016/0021-9991(90)90196-8

[6] Gresho, P., "Incompressible Fluid Dynamics: Some Fundamental Formulation Issues," *Annual Review of Fluid Mechanics*, Vol. 23, No. 1, 1991, pp. 413–453. doi:10.1146/annurev.fl.23.010191.002213

[7] Roache, P., *Verification and Validation in Computational Science and Engineering*, Hermosa Publishers, Socorro, New Mexico, 1998.

[8] Abbott, I., and Von Doenhoff, A., *Theory of Wing Sections: Including a Summary of Airfoil Data*, Dover Publications, New York, 1959.

[9] Selig, M., and Guglielmo, J., "High-Lift Low Reynolds Number Airfoil Design," *Journal of Aircraft*, Vol. 34, No. 1, 1997, pp. 72–79. doi:10.2514/2.2137

[10] Liu, T., Kuykendoll, K., Rhew, R., and Jones, S., "Avian Wings," *AIAA 24th Aerodynamic Measurement Technology and Ground Testing Conference*, Portland, Oregon, AIAA Paper 2004-2186, June 2004.

[11] Taylor, G., Nudds, R., and Thomas, A., "Flying and Swimming Animals Cruise at a Strouhal Number Tuned for High Power Efficiency," *Nature*, Vol. 425, 2003, pp. 707–711. doi:10.1038/nature02000

[12] Young, J., and Lai, J., "Mechanisms Influencing the Efficiency of Oscillating Airfoil Propulsion," *AIAA Journal*, Vol. 45, No. 7, 2007, pp. 1695–1702. doi:10.2514/1.27628

[13] Wang, Z., "Vortex Shedding and Frequency Selection in Flapping Flight," *Journal of Fluid Mechanics*, Vol. 410, 2000, pp. 323–341. doi:10.1017/S0022112099008071

M. Visbal
Associate Editor